Raman identification of the different glazing technologies of Blue-and-White Ming porcelains

Philippe Colomban, Anh-Tu Ngo, Howell G.M. Edwards, Linda C Prinsloo, L. Valérie Esterhuizen

Raman identification of the different glazing technologies of Blue-and-White Ming porcelains

Philippe Colomban[1*], Anh-Thu Ngo[1], Howell G.M. Edwards[2], Linda C Prinsloo[3], L. Valérie Esterhuizen[4]

[1] Sorbonne Université, CNRS, MONARIS umr8233, 4 Place Jussieu, 75005 Paris, France

[2] School of Chemistry and Biosciences, Faculty of Life Sciences, University of Bradford, Bradford, West

Yorkshire BD18 4JX, United Kingdom

[3]Evolutionary Studies Institute, University of the Witwatersrand, PO WITS 2050, South Africa.

[4]Independent researcher, 287 Pleiades Ave, Waterkloof Ridge, Pretoria, 0181

*corresponding author philippe.colomban@sorbonne-universite.fr

Fax +331 44272731

Tel + 33144272785

Highlights

- Raman and SEM-EDS evidence of Ca-rich and Ca-poor glaze of Blue-and-White Ming porcelain from shipwrecks of Portuguese ships.

- The blue decoration is either placed under-glaze, or in-glaze as found in the Vietnamese productions of the same period.

- Previous assignments of the Raman signature of feldspar to cobalt aluminate are now not favoured.

Raman identification of the different glazing technologies of Blue-and-White Ming porcelains

Philippe Colomban[1*], An-Thu Ngo[1], Howell G.M. Edwards[2], Linda C Prinsloo[3], L. Valérie Esterhuizen[4]

[1] Sorbonne Université, CNRS, MONARIS umr8233, 4 Place Jussieu, 75005 Paris, France

[2] School of Chemistry and Biosciences, Faculty of Life Sciences, University of Bradford, Bradford, West Yorkshire BD18 4JX, United Kingdom

[3] Evolutionary Studies Institute, University of the Witwatersrand, PO WITS 2050, South Africa.

[4] Independent researcher, 287 Pleiades Ave, Waterkloof Ridge, Pretoria, 0181

*corresponding author philippe.colomban@sorbonne-universite.fr

Fax +331 44272731   Tel + 33144272785

Abstract

Shards of Blue-and-White Ming porcelain from shipwrecks of Portuguese ships found on the coasts of South Africa plus a shard from Mombasa (Kenya) were analyzed by optical microscopy, SEM-EDS and Raman microspectroscopy (458 nm). Whereas the Raman signature of porcelain body paste compositions which are based on mullite, quartz and an amorphous phase with the minor presence of anatase and feldspar are very comparable whatever the variable alumina content, at least two types of glazes are observed: a high-temperature soda-potassium glaze, and glazes richer in calcium and similar to a celadon glaze (with the possibility of wollastonite formation). The blue decoration is obtained with a material rich in manganese typical of the Ming productions. Some shards exhibit a two-layer glaze and the blue decoration is either placed under-glaze, or in-glaze as found in the Vietnamese productions of the same period. Previous assignments of the Raman signature of feldspar to cobalt aluminate are now not favoured (blue colour is obtained with Co^{2+} ions dissolved in the glassy silicate) and several black spots exhibit the characteristic spectrum of an epsilon Fe_2O_3 phase being present.

Keywords : porcelain ; glaze ; blue ; cobalt ; composition ; Raman microspectroscopy ;

1. Introduction

Shipwreck cargoes are archaeological time capsules as any object in the cargo could only have been produced before the ship left shore and if the date that the ship sank is known, it provides some evidence for the production date of the artefacts. This is the case for the shipwrecks from which the shards studied here were selected[1-3]. Similar shards have already been studied summarily or with illumination conditions (785 nm)[4,5] under excitation which did not make it possible to characterize all the phases present as is the case when blue laser excitation is employed as has been done here. The work presented here, by coupling Raman analysis with SEM-EDXS analysis, allows the characterization of the elemental composition and to identify the molecular signatures of the constituent phases of the paste and the enamels. We illustrate how non-invasive Raman microspectroscopy analysis allows a rapid categorization of the different types of porcelain according to the nature of the enamel used. The observation of the stratigraphy makes it possible to discuss decoration techniques and in particular to check whether, as is commonly reported, the blue-and-white decorations are placed underglaze or, as in many contemporary Vietnamese productions of the Ming Dynasty, are placed overglaze on the enamel.[6] Indeed, the study of the blue-and-white Vietnamese porcelains produced along the Hong River (Hai Dung Province) showed that porcelains from neighbouring kilns were produced with chemically different enamels which were nevertheless visually, very similar[7]. It was interesting to analyze in the current work a range of porcelain shards obtained from shipwrecks and to try to correlate the different types with the characteristics of the manufacturing productions employed in the different Chinese kilns. Raman microspectroscopic analyses of pottery can now be performed on-site non-destructively,[8,9,10] which allows the study of rare and preserved artefacts and provide information and knowledge about the production technology more statistically.

2. Experimental

2.1. Specimens

Vasco da Gama opened the maritime route from Europe to India around the Cape of Good Hope (known as Carreira da India) in 1498 making it possible for Portuguese ships to travel around the Cape of Good Hope to the East on a regular basis transporting valuable cargoes of Eastern spices, carnelian beads and Chinese porcelain to Europe on their return journeys. However, the route around the Cape is infamous for its stormy weather and treacherous seas and at least fifteen Portuguese galleons on the Carreira da India route suffered casualties along the South African shores before 1686 AD. Nine of these wrecks (dating between 1552 and 1647) are associated with numerous Chinese porcelain shards that with time found their way to beaches along the South African shores closest to the shipwreck sites.[1,3] This provides a large number of Ming porcelain shards from Jiajing and Wanli reigns (collected over several years by various people) that makes it possible to study changes in aspects of production technology and decorative motifs of Chinese porcelain over a period of nearly one century

The following specimens were acquired from this cache for comparative analytical purposes: comprising a group of shards, glazed and decorated in blue (Table 1 and Figure 1), collected by Dr Valerie Estherhuizen[1-3] : i) the São Jão shipwreck (1552) collected at Port Edward and Port Shepstone (the two places being distant some ~40 km along the Southern Natal coast but it is suspected that the shards are coming from the same cargo; ii) the Santo Alberto shipwreck (1593) collected at Morgans Bay and Haga Haga, Eastern Cape; iii) the Santa Maria Madre de Deus shipwreck (1643), at Bonza Bay, East London; and iv) the Nostra Senhora da Atalaya do Pinheiro shipwreck (1647), Kefane, north of East London. The shard collected at Mombasa (1630?) belongs to a Kraak ware type and matches closely the shard #b4 from the Santa Maria Madre de Deus (Fig. 1). Similar shards have been previously studied by Raman microspectroscopy by De Waal[2] and Carter et al.[3] but using different experimental conditions.

2.2. Spectroscopic instrumentation

Raman spectroscopic analyses were carried out using firstly a high sensitivity LABRAM Infinity Dilor spectrometer equipped with a 532 nm JDS-Uniphase YAG laser and a HORIBA Jobin-Yvon Peltier cooled CCD and, secondly, a high resolution HR800 HORIBA Jobin-Yvon spectrometer equipped with similar CCD detector but illuminated with a Coherent Innova 90C Ar^+ ion laser (from which the 458 nm excitation line was used) in order to obtain a global view of the different Raman spectral signatures. The laser power is about 3 to 5 mW at the sample using the 458 nm line excitation and 0.5 mW for 532 nm excitation. Backscattering measurements are made with Olympus Long Working Distance x 50 and x 100 objectives. Between 5 to 10 different replicate spots were analysed for each shard specimen in section and at the glazed surface to achieve a representative survey (recording times: 2 to 10 min per spectrum, typically). Due to the large fluorescence observed under 532 nm excitation a base line subtraction is required for spectra recorded with the LABRAM instrument (see Figure S1, Supplementary Materials). In contrast, the spectra recorded with the 458 nm laser line exhibit fluorescence only above ~1200 cm^{-1} and these as-recorded spectra will be presented without baseline correction in the present paper. Similar phases were observed with both instruments.

2.3. *SEM-EDS*

It turned out to be advantageous to make a notch on each of the fragments with a diamond saw (Minitom, Struers) and to further break the shard with pliers to have a fresh fracture, which was then observed with a BX51 Olympus Microscope (Fig. 2), for both the Raman and SEM analyses. Elemental composition of each shard section was obtained using a JEOL 5510LV SEM-EDXS (IXRF Systems 500 digital processing) spectrometer with an acceleration voltage of 20 kV. In order to limit detrimental charge effects, the sample was partially wrapped with a carbon-rich tape having an observation window clear for the area to be analyzed. The charge evacuation is not as good as with the application of a conducting coating (C or Au-Pd) but the samples are better preserved for Raman

analysis. Furthermore, due to the difficulty of recognizing specific coloured areas on SEM images, the window helps to correlate a comparison between the Raman and SEM-EDXS measurements. EDXS spectra were recorded using low magnification in order to acquire data representative of the materials under interrogation (the sample areas measured are ~200x 400 μm^2 for the body and ~100x200 μm^2 for glaze. It is important to note that, unlike coloured glass, coloured pigment enamels are heterogeneous at the scale of a few microns. Quantitative elemental analysis (oxide wt %) was achieved using the ZAF calculation method as implemented in the Iridium Ultra software. The validity of the measurements was monitored by applying the same procedure to certified glass-reference samples: namely, "Corning Museum B, C and D" and American "National Bureau of Standard (NBS 620)" and the error is estimated to be less than 10% for most of the measured elements. It should be noted that boron cannot be measured in these experiments.

3. Results

3.1. Microstructure and stratigraphy

Fig. 1 shows the set of shards that were the subject of the analytical study here. Sections of the most specific shards are presented in Fig. 2. Table 1 summarizes the information regarding the provenance, the gloss of the glazes observed and the colour of the body. Three types can be distinguished by this visual examination: the shard from the São Jão (Port Edward) exhibits a greenish body as well that labelled a1 from the Santa Maria Madre de Deus shipwreck. The other bodies are white. The shards from the Nostra Senhora shipwreck and from São Jão Port Edward are thicker (~11.5 and 4.5 mm, respectively to be compared with a thickness ranging from ~2 to 3 mm for the others); the Nostra Senhora shard shows many cracks. The shards labelled SMMD b1 and b3 seems experienced more glaze corrosion and the blue pigment decoration is paler than the others. Two shards exhibit a glossy glaze, namely, the specimen from Mombasa (Fig 1a) and the one labelled 4

from the Santa Maria Madre de Deus shipwreck (Fig. 1b). The high gloss is also obvious visually correlated with the more concoïdal character of the fracture (Fig. 2). The thickness of the glaze ranges between 200 and 300 µm. The highest concentration of blue pigment is clearly observed at the glaze-body interface for shards from the São Jão (Port Shepstone), Nostra Senhora, Santo Alberto b and Mombasa. It is difficult to conclude anything in this respect for the other Santo Alberta shard. In contrast, for the São Jão (Port Edward) and Santa Maria Madre de Deus a4 shards the homogeneous blue colour of the glaze section and the sharp white body-blue glaze interface are strongly indicative for the drawing of the blue decoration on the glaze precursor layer (inglaze blue). Examination of the Mombasa shard section shows a change of the glaze microstructure close to the surface on about the scale of a 25 µm thick layer. The surface of some other shards (e.g. the Santo Alberto b shard, Fig. 2) also shows some modification close to the surface, which can be most likely ascribed to corrosion.

3.2. Body composition and phases

EDXS spectra of the body, colourless glaze and blue glaze of representative samples are reported in the supplementary materials (Figures S2 to S4), while the analysis data are given in Table 2..

As expected for porcelain, a rather large content of aluminium (~20 to 25 Al_2O_3 wt%) is measured as well as potassium (1 to 2 K_2O wt%), sodium (1 to 3 Na_2O wt%) and calcium (2 to 7 CaO wt %) with minor amount of magnesium (0.5 to 1 MgO wt %). The relatively high level of sodium may result from marine pollution (Table 2). The small differences obviously may be ascribed to the variability of the production and the medium accuracy of the procedural measurement and a statistical study is required to compare precisely the results. As shown in Fig. 3 the spectra of mullite with characteristic peaks at 270, 320, 415, 605, 710, 875, 960 and 1135 cm^{-1} [11] and of quartz (120, 200, 260, 460, 690, 795, 1065 and 1150 cm^{-1})[12] are obtained in many replicate spots sampled. Feldspar or plagioclases (main peak at ~500 to 515 cm^{-1})[13-16] are also observed in some spots. Different feldspar/plagioclases signatures are recorded showing a poor-resolved triplet close to 505 cm^{-1} (Low-temperature

anorthite, $CaAl_2Si_2O_8$) to a well-resolved triplet with a maximal peak at ~513 cm^{-1} (microcline, $MAlSi_3O_8$; M = K, Na, …) that arises from a variable composition and to the modification induced by the firing process. Presence of sanidine and anorthoclase is also possible. The signature of the amorphous glassy phase of porcelain (a strong broad band at 485 cm^{-1}, with weaker and broad bands at 585, 790, 1010 and 1120 cm^{-1})[17,18] is also well observed for all samples, and these features are generally associated with mullite peaks. It is rather difficult to record a "single phase" spectrum, even with the x100 microscope objective (spot diameter <3 μm). This is consistent with the formation of a mass of mullite needles to form the rigid network hosting the molten phase during the firing. The carbon doublet (~1375-1590 cm^{-1}) is observed for all shards in some spots (see e.g. in Fig. 3) that is consistent with a firing under a reducing atmosphere in the kiln (as requested to obtain a blue décor using Asian (Mn-rich) cobalt). The low intensity of the doublet indicate concentration less than 0.5 wt%. Iron oxide ranges between # 0.2 and 0.7 % as usually found for Ming porcelain. Unusual phases are detected in the Nostra Senhora and Mombasa shards with the presence of calcium carbonate (1085 cm^{-1}, Fig. 3) and gypsum (1007 cm^{-1}). Similar features were reported by de Waal[4,] also for a shard from the Santa Maria Madre de Deus shipwreck. Pollution from the marine environment that would result in calcite/aragonite and sulfates (bio)deposits is likely for these exemplars.[19] The Raman signature of anatase (TiO_2), a common impurity of clays/kaolin, is also observed in the Mombasa, Santo Alberto (both groups), Santa Maria Madre de Deus b4, and São Jão shards.

Chlorine is detected elementally in some bodies and in some glazes (Table 2 and Figures S2-S4, Supplementary Materials) and this is likely to occur due to the presence of NaCl residues in the cracks from immersion of the shards in sea water, which has not been fully eliminated by washing.

It is noticeable that the SiO_2 content for the porcelain body of the oldest sample (São Jão) is 70-75%, and roughly decreases over time to 64% for the Mombasa sample (Table 2), while the Al_2O_3 content increases from ~20% to ~30% during the same time period. This might be an indication that the clay recipe for the porcelain body have changed over time to adjust to commercial kilns that produced

mainly *Kraak* ware that specially made for the export market. Up to 1600, Portuguese ships did not reach China, but sourced Chinese porcelain from sites in India, after 1600 they obtained porcelain directly from China. So difference in clay and glaze recipes could also be due to technology differences between different kilns. However, a study of a larger number of samples is necessary to make any positive deduction.

3.3. Glazes

Although differences between the porcelain bodies are subtle and are not easily identified by Raman scattering, at least two types of glaze are readily identified in the shard specimens both by SEM-EDS and by Raman microspectroscopy. Comparison of the relative intensity of the EDS peaks characteristic of potassium and calcium gives also a visual comparative evidence of these two types: the K and Ca peaks have a similar intensity for all the other shards except for the shard samples from the São Jão, the Santa Maria Madre de Deus b1 and b4, and for the Nostra Senhora shard, for which the Ca peak is stronger than that of K (Figures S2-S4, Supplementary Materials). This is also evident from the difference in composition (Tables 2b and 2c).

The different Raman signatures are summarized in Figure 4. Ca-rich glazes exhibit a strong broad SiO_4 stretching band peaking from 975 to 990 cm^{-1} with an additional component, which may be more or less strong at 1120-1130 cm^{-1}. The bending SiO_4 (broad) band peaks at about 500 cm^{-1} and exhibits a slightly smaller intensity. These spectra are rather similar to those recorded on Vietnamese porcelain shards from the Cù Lào Cham Island shipwreck (15th Century, close to the Hôi An port city) and from the My Xa kiln (Hai Duong Province)[7] and can be also related to the signature recorded on 14th century (Vietnamese) celadons.[20] The thermal analyse of these Vietnamese shards demonstrated that they were fired between ~1250°C (Ca-rich glaze) and ~1350°C or more (Ca-poor glaze). For the glazes that exhibit similar intensity for the main K and Ca EDXS peaks, the Raman spectra show a strong broad band at ca. 480 cm^{-1} (plus in many cases a superimposition of the narrow quartz peak at ~465 cm^{-1}) and much smaller broad bands at ~790, 1050 and 1120 cm^{-1}. These spectra are similar to those

recorded from Meissen and other hard-paste European porcelain glazes and are characteristic of a high-temperature fired glazed porcelain.[17,18,21]The estimate of the polymerization index from the ratio of the area of the bands of the SiO_4 bending modes compared to that of stretching modes according to Colomban et al.[21] gives indices of ~1.5 and 3 for the glazes respectively rich and poorer in calcium.

Narrow peaks characteristic of crystalline phases are also recorded in the Raman spectra : i) those of feldspar/plagioclases (a narrow 515 cm^{-1} peak characteristic of a K-rich microcline to a broader ca. 505 cm^{-1} peak characteristic of a Ca-rich low-temperature anorthite phase, Fig. 4)[14] and ii) those of $CaSiO_3$ beta wollastonite (characteristic doublet at 635 and 968 cm^{-1}, Fig. 4).[21-24] Beta wollastonite is a characteristic phase of soft-paste European porcelain glaze and body rich in calcium which have been fired at lower kiln temperatures.[21-23]

3.4. Blue decoration

Figure 5 shows representative spectra recorded from the blue/dark blue decoration, including some rare black spots. In most of the spots analyzed no differences are observed between the spectra recorded from the colourless and blue glazes, wherever the focus, close to the glaze surface or in the glaze itself (carried out on measurements on the shard surface or on its section). This implies that blue colour results from the dissolution of Co^{2+} ions within the glaze, without formation of crystalline Co-based phase. Compositions (Tables 2b and 2c) are also similar, except regarding Mn, Co and Fe content. In rare cases, the signature of plagioclase or of wollastonite is observed for certain specimens, as reported above (see also further paragraph). Two additional types of Raman spectra are also observed and reported here. The spectrum (Fig. 5) of black spots (Fig. 6) is characteristic of an exotic iron oxide phase, epsilon-Fe_2O_3, with characteristic bands at ca. 400, 505, 555, 655, and 745 cm^{-1}.[25-27] Epsilon-Fe_2O_3 has been recently recognised in many glazes of Asian pottery.[25-30] As shown in Fig. 6, these black spots are formed in relation with a bubble. Dendrites are usually present, formed

11

at the liquid/gas interface. A second unusual spectrum is recorded also: a strong, broad band at ~685 cm^{-1} associated with a smaller 850 cm^{-1} peak. The strong ~685 cm^{-1} band fits well with a spinel phase,[31,32] according to the observed measurement of manganese and iron (Table 2c), as characterized also on Ming blue-and-white porcelains by Pinto et al.[25] The peak at 850 cm^{-1} is consistent with a phase comprising CrO_4 entities[32] as observed when chromite is used in the pigment preparation.[33] Chromium is, however, often present and found in cobalt ores.[27]

The calcium content is higher in blue glaze than in coloured glaze for some shards (São Jão PE, Santa Maria Madre de Deus a1 and b1), especially close to the surface.

Contrary to some previous assignments[4,34,35] of the ca. 505 cm^{-1} to a $CoAl_2O_4$ phase the presence of other peaks characteristic of plagioclases (e.g. at about 160,285 and 635 cm^{-1}, Fig. 4) and the absence of the stronger (and narrow) peak of $CoAl_2O_4$ at 200 cm^{-1} is fully consistent with the absence of the $CoAl_2O_4$ signal as reported by Pinto et al.[25] and by Colomban et al.[27] The higher ionicity of the Al-O bond in comparison with the Si-O bond means that even if cobalt aluminate and silicates are simultaneously present in similar amounts, the Raman spectrum will only reveal the silicate phase.[37-39] A careful microdiffraction study of Pinto et al. commonly identified $CoFe_2O_4$ and exceptionally $CoAl_2O_4$.[39,40] Partially substituted cobalt aluminate was also identified by Wang et aL. using Synchrotron μXRD.[41]

3.5. Body-glaze interface

Figure 7 shows the sequence of Raman spectra recorded on the section of representative shards of each type along a line transect from the centre of the porcelain body up to the glaze surface (Ca low, medium and rich glazes are chosen). A variety of spectra of plagioclases, with the stronger peak ranging from 505 (anorthite) to 515 cm^{-1} (microcline) which is very narrow in bandwidth (see also Fig. 5 bottom spectrum) is observed at the interface between the mullite-rich paste and the glaze, indicating the formation of these phases after the reaction between the molten glaze and the body. Residual quartz grains remain both in the body, glaze and at the interface.

4. Discussion

The two classes of Ming blue-and-white glaze, Ca-rich and Ca-poor have been already identified by Zhang in a seminal review on the glazing technology of Chinese pottery[42] and more recently by Wen et al.[34] in the study of similar shards excavated from the Shangchuan Island (Guangdong Province), an active trading port during 16th century (Zhengde and Jiajing periods of the Ming Dynasty) hosting Portuguese ships. Under-glaze and in-glaze décor were also observed by Wen et al. for one of the three shards studied in their paper, all three being assigned to have been produced at Jingdezhen. Wen et al.[34] suggest that the blue drawing was made on a body already covered with glaze powder (overpainted décor) and that a second deposition of the glaze powder precursor was made before firing. This would explain the homogeneous dispersion of the blue colour in the glaze (in-glaze blue) and not its concentration at the body-glaze interface as observed for Mombasa specimen (Fig. 2). We have compared the amount of transition metals found for our different shards: only for Santa Maria Madre de Deus a4 does the interface region show a higher content in manganese, characteristic of an underglaze décor ; indeed, due to the much higher colouring power of cobalt for glazes fired under reducing conditions, blue decoration can be obtained using Asian impure cobalt ores, which are rich in Mn and Fe, and in many cases they are found to be richer than they are in Co.[6,27,43] Dark blue colours were obtained with cobalt ores exhibiting a medium content of manganese (Table 2c). This can be the proof of the use of different cobalt grades, as previously reported.[27,44] The diffusion of blue colour within the paste as clearly visible on the photomicrographs in Fig. 2 for the São Jão PS, Nossa Senhora, Santo Alberto b and Mombasa shards confirms that the drawing of the blue decoration was made for these specimens on the unfired (green) body and the glaze powder precursor deposited upon it before the firing.

Double-layer glazing was claimed by Wen et al. from a cross-sectional image for one shard and explained on the basis of a double glazing step, as reported for the Fujian (Zhangzhou) kilns by Zhou

et al.[45] and Zhang et al.[46] If a double-layer could be recognized on the Mombasa and one of the Santo Alberto(b) shards (Fig. 2) it would be difficult to assign this feature to a double glazing step and it is likely this can be ascribed to the marine corrosion at least for San Alberto (b) shards. We have attempted but not succeeded in characterising different Raman signatures for glaze sections compatible with a double layered glazing process. A rather strong fluorescence signal starts above 1000 cm^{-1}, especially when the spectral recording is made at the glaze surface. This is consistent with the presence of a fluorescence emission related to bio-corrosion. It is possible that a polishing and an annealing treatment undertaken at a temperature in the 600-800°C range (a temperature sufficiently high enough to burn out organic residues yet sufficiently low to avoid any modification resulting to the inorganic phases) would eliminate the fluorescence induced by the bio-film formed in the marine environment with long immersion with more efficiency than the blue laser illumination and therefore allow a more precise study of the stratigraphy of the glazes.

Zhang et al.[46] showed that the presence of double-layered glazing existed for *Kraak* wares. Element distribution mapping clearly showed that the surface glaze layer is richer in calcium, as we have observed her for some blue decoration (we observe similar feature Fig. S2, São Jão PE and Fig. S4, Mombasa, Supplementary Materials). However for most of the samples they studied they could not detect cobalt. The Raman spectra of Zhang et al.[46] were recorded using the 785 nm laser line excitation, that could not permit the detection of the vibrational signature of the Si-O network, but only fluorescence emission and consequently their assignment and conclusions derived from their Raman spectra are rendered irrelevant: they assign the 1350 cm^{-1} feature which is really a fluorescence band, already observed in ref. 3 (spectra also recorded with 785 nm excitation), to the asymmetric stretching vibration of SiO_4 tetrahedra although only the symmetrical stretching modes contribute significantly to Raman scattering and these are located between ~850 and 1100 cm^{-1} according the degree of polymerization of the silicate matrix.[36-38] Obviously, more analyses are needed to document better the differentiation between the final products of the glazing procedure, namely single or multiple steps, especially using non-invasive spectroscopic techniques.

Nevertheless, the calculation of the polymerisation indices directly linked to the melting temperature of the vitreous silicates[21,36-38] shows that the two types of enamels (alkaline or rich in calcium) have been fired at different temperatures The double glazing technique could explain why *Kraak* wares[47,48] from shipwrecks maintain their high gloss although other porcelain samples become pitted and gloss-free.

5. Conclusions

The combination of SEM-EDS and Raman microspectroscopy is efficient to categorize shards in a non-invasive way if the pieces are sufficiently small to be put in an SEM chamber. Access to the section/fracture is required for a good analysis to be performed. A freshly made fracture is sufficient to permit access to un-corroded material and the use of blue (or even better a violet laser excitation line) is required to fully characterize the vibrational signatures of silicates, crystalline (mullite, feldspar/plagioclases, quartz, wollastonite) and amorphous (glaze). If a green laser line is used, subtraction of a baseline is required to identify all signatures. Two groups of glazes are unambiguously identified here in the present study: namely a Ca-rich glaze (the saturation in calcium leads to the precipitation of beta wollastonite) linked to the glaze of celadons and fired at temperatures close to 1200-1250°C and a mixed Na-K-Ca glaze fired at a higher temperature. More specimens should be analyzed with this procedure to identify the list of specifications that should be recorded for the further identification of the kiln of origin. The Raman spectrum unambiguously identifies the two types of glaze.

Declaration of competing interest

The authors declare that they have no known competing financial interests or personal relationships that could have appeared to influence the work reported in this paper.

References

1. L.V. Esterhuizen, History written in porcelain sherds. The São João and the São Bento, two 16th century Portuguese shipwrecks, Taoci 2 (2001) 111-116.

2. L.V. Esterhuizen, Dekoatiewe Motiewe op Chinese Porseleinkerwe uit Portugese Skeepswrakke aan die Suid-Afrikaanse Kus 1552-1647, PhD, Universiteit van Pretoria, Pretoria, 2001.

3. A. Meyer, L.V. Esterhuizen, A southern African perspective of the early Indian Ocean trade, ch. 4 in Maritime Contacts of the Past. Decephering Connections Amonst Communities, S. Tripati, Ed. Delta Book Word, New Delhi, India, 2015,pp. 54-94.

4. D. de Waal, Raman investigation of ceramics from 16th and 17th century Portuguese shipwrecks, J. Raman Spectrosc. 35 (8-9) (2004) 646-649. https://doi.org/10.1002/jrs.1210

5. E.A. Carter, M.L. Wood, D. de Waal, H.G.M. Edwards, Porcelain shards from Portuguese wrecks: Raman spectroscopic analysis of marine archaeological ceramics, Herit. Sci. 5 (2017) 17. https://doi.org/10.1186/s40494-017-0130-9

6. G. Simsek, P. Colomban, S. Wong, B. Zhao, A. Rougeulle, N.Q. Liem, Toward a fast non-destructive identification of pottery: The sourcing of 14th-16th century Vietnamese and Chinese ceramic shards, J. Cult. Herit. 16 (2) (2015) 159-172. DOI:10.1016/j.culher.2014.03.003

7. P. Colomban, N.Q. Liem, G. Sagon, H.X. Tinh, T.B. Hoành, Microstructure, composition and processing of 15th century Vietnamese porcelains and celadons, J. Cult. Herit. 4 (3) (2003) 187-197.DOI:10.1016/S1296-2074(03)00045-1

8. P. Colomban, F. Ambrosi, A.-T. Ngo, T.-A. Lu, X.-L. Feng, S. Chen, C.L. Choi, C. Comparative Analysis of Wucai Chinese Porcelains Using Mobile and Fixed Raman Microspectrometers. Ceram. Int. *43* (16) (2017) 14244–14256. https://doi.org/10.1016/j.ceramint.2017.07.172

9. P. Colomban, On-site Raman study of artwork: Procedure and illustrative examples, J. Raman Spectrosc. 49 (6) (2018) 921-934. https://doi.org/10.1002/jrs.5311

10. P. Colomban, B. Kırmızı, B. Zhao, J.-B. Clais, Y. Yang, V. Droguet, V. Investigation of the Pigments and Glassy Matrix of Painted Enamelled Qing Dynasty Chinese Porcelains by Noninvasive On-Site Raman Microspectrometry, Heritage 3 (3) (2020) 915–940. https://doi.org/10.3390/heritage3030050

11. D. Michel, P. Colomban, S. Abolhassani, F. Voyron, A. Kahn-Harari, Germanium mullite: Structure and vibrational spectra of gels, glasses and ceramics, J. Eur. Ceram. Soc. 16 (2) (1996) 161-168.

12. J.F. Scott, S.P.S. Porto, Longitudinal and transverse optical lattice vibrations in quartz, Phys. Rev. 161 (1967) 903-910.

13. D.W. Matson, S.K. Sharma, J.A. Philpotis, Raman spectra of some tectosilicates and glasses along orthoclase-anorthite and nepheline-anorthite joins, Amer. Mineral 71 (5-6) (1986) 694-704.

14. J.J. Freeman, A. Wang, K.E. Kuebler, B.L. Jolliff, L.A. Haskin, Characterization of natural feldspars by Raman spectroscopy for future planetary exploration, The Can. Mineralogist 46 (6) (2008) 1477-1500. DOI:10.3749/canmin.46.6.1477

15. L.C. Prinsloo, P. Colomban, J.D. Brink, I. Meiklejohn, Raman spectroscopic study of the igneous rocks on Marion Island: a possible terrestrial analogue for the geology on Mars, J. Raman Spectrosc., 42 (4) (2011) 626-632. DOI: 10.1002/jrs.2756

16. D. Bersani, I. Aliatis, M. Tribaudino, L. Mantovani, A. Benisek, M.A. Carpenter, G. Diego Gatta, P.P. Lottici, Plagioclase composition by Raman spectroscopy, J. Raman Spectrosc., 49 (4) (2018) 684-698. DOI: 10.1002/jrs.5340

17. P. Colomban, F. Treppoz, Identification and differentiation of ancient and modern European porcelains by Raman macro- and micro-spectroscopy, J. Raman Spectrosc. 32 (2) (2001) 93-102. DOI: 10.1002/jrs.678

18. P. Colomban, V. Milande, On-site Raman analysis of the earliest known Meissen porcelain and stoneware, J. Raman Spectrosc. 37 (5) (2006) 606-613. DOI : 10.1002/jrs.1494

19. J. Du, W. Luo, N. Li, C. Wang. Characterization of the micro-contaminants from the inner-body of Kraak porcelain, excavated from the "Nan'ao" shipwreck, the South China sea, Herit. Sci. 7 (1) (2019) 85. DOI:10.1186/s40494-019-0328-0.

20. N.Q. Liem, N.T. Thanh, P. Colomban, Reliability of Raman micro-spectroscopy in analysing ancient ceramics: the case of ancient Vietnamese porcelain and celadon glazes, J. Raman Spectrosc. 33 (4) (2002) 287-294. DOI: 10.1002/jrs.854

21. P. Colomban, I. Robert, C. Roche, G. Sagon, V. Milande, Identification des porcelaines "tendres" du 18ème siècle par spectroscopie Raman: Saint-Cloud, Chantilly, Mennecy et Vincennes/Sèvres, Revue d'Archéomètrie 28 (2004) 153-167.

22. J. Partyka, M. Lesniak, Raman and infrared spectroscopy study on structure and microstructure of glass-ceramic materials from SiO_2-Al_2O_3-Na_2O-K_2O-CaO system modified by variable molar ratio of SiO2/Al2O3, Spectrochim. Acta Part A: Mol. & Biomol. Spectrosc. 152 (2016) 82-91. DOI: 10.1016/j.saa.2015.07.045

23. P. Colomban, M. Gironda, H.G.M. Edwards, The Enamels of the First (Soft-paste) European Blue-and-white Porcelains: Rouen, Saint-Cloud and Paris Factories: Complementarity of Raman and X-ray Fluorescence analyses with Mobile Instruments to identify the cobalt ore, J. Raman Spectrosc. 2022, DOI: 10.1002/jrs.6111.

24. RRUFF data base, ref R0400131, https://rruff.info/Wollastonite/R040131 (accessed 5th July 2021).

25. A. Pinto, P. Sciau, T.Q. Zhu, B. Zhao, E.S. Groenen, Raman study of Ming porcelain dark spots: Probing Mn-rich spinels. J. Raman Spectrosc. 50 (5) (2019) 711–719. DOI : 10.1002/jrs.5568.

26. J. López-Sánchez, A. Serrano, A. Del Campo, M. Abuín, O. Rodríguez de La Fuente, N. Carmona, Sol-gel synthesis and micro-Raman characterization of ϵ-Fe_2O_3 micro- and nanoparticles. Chem. Mater. 28 (2) (2016) 511–518. DOI : 10.1021/acs.chemmater.5b03566

27. P. Colomban, G. Simsek, B. Kirmizi, Cobalt and Associated Impurities in Blue (and Green) Glass, Glaze and Enamel: Relationships between Raw Materials, Processing, Composition, Phases and International Trade, Minerals 11 (6) (2021) 633. https://doi.org/10.3390/min11060633

28. Q.Y. Hoo, Y.H. Liang, X.L. Yan, X.H. Wang, T.W. Cao, X.W. Cao, Millimeter-sized flower-like clusters composed of mullite and ε-Fe_2O_3 on the Hare's Fur Jian Ware. J. Eur. Ceram. Soc. 40 (12) (2020) 4340–4347. DOI :10.1016/j.jeurceramsoc.2020.04.032

29. Z. Liu, C. Jia, L. Li, X. Li, L.Y. Ji, L.H. Wang, Y. Lei, X.J. Wei, The morphology and structure of crystals in Qing Dynasty purple-gold glaze excavated from the Forbidden City. J. Am. Ceram. Soc. 101 (11) (2018) 5229–5240. DOI :10.1111/jace.15759

30. Y. Kusano, T. Fujii, J. Takada, M. Fukuhara, A. Doi, Y. Ikeda, M. Takano, Epitaxial growth of ε-Fe_2O_3 on mullite found through studies on a traditional Japanese stoneware. Chem. Mater. 20 (1) (2008) 151–156. DOI :10.1021/cm7023247

31. Z. Cvejic, S. Rakic, A. Kremenovic, B. Antic, C. Jovalekic, P. Colomban, Nanosize ferrites obtained by ball milling: Crystal structure, cation distribution, size-strain analysis and Raman investigations, Solid State Sci. 8 (8) (2006) 908-915. DOI :10.1016/j.solidstatesciences.2006.02.041

32. P. Colomban, G. Sagon, X. Faurel, Differentiation of antique ceramics from the Raman spectra of their coloured glazes and paintings, J. Raman Spectrosc. 32 (5) (2001) 351-360. DOI :10.1002/jrs.996

33. P. Colomban, V. Milande, L. Le Bihan, On-site Raman analysis of Iznik pottery glazes and pigments, J. Raman Spectrosc. 35 (7) (2004) 527-535. DOI :10.1002/jrs.1163

34. J.X. Wen, Z.K. Chen, Q.G. Zeng, L.S. Hu, B. Wang, J.P. Shi, G.X. Zhang, Multi-micro analytical studies of blue-and-white porcelain (Ming dynasty) excavated from Shuangchuan island, Ceram. Int. 45 (10) (2019) 13362-13368. DOI :10.1016/j.ceramint.2019.04.031

35. X.C.Y. Jiang, Y.Y. Ma, Y. Chen, Y.Q. Li, Q.L. Ma, Z.X. Zhang, C.S. Wang, Y.M. Yang, Raman analysis of cobalt blue pigment in blue and white porcelain: a reassessment, Spectrochim. Acta Part A-Mol. & Biomol. 190 (2018) 61-67. DOI :10.1016/j.saa.2017.08.076

36. P. Colomban, Glaze and enamels. In *Encyclopedia of Glass Science, Technology, History and Culture*; 1st ed.; Richet, P., Ed.; John Wiley and Sons, Inc.: Hoboken, NJ, USA, 2020, pp. 1309–1326.

37. P. Colomban, O. Paulsen, Non-destructive Raman Determination of the Structure and Composition of Glazes by Raman Spectroscopy. *J*. Amer. Ceram. Soc. 88 (2) (2005) 390–395. DOI :10.1111/j.1551-2916.2005.00096.x

38. V. Labet, P. Colomban, Vibrational properties of silicates: A cluster model able to reproduce the effect of "SiO_4" polymerization on Raman intensities. J. Non-Crystall. Solids 370 (2013) 10–17. DOI :10.1016/j.jnoncrysol.2013.03.025

39. A. Pinto, Microstructure et procédés techniques des porcelains *qinghua*: Une approche de type Science des Matériaux. PhD Thesis, Université de Toulouse, Toulouse, France, 10 October 2019. Available online: http://www.theses.fr/2019TOU30183 (accessed on 5th January 2021).

40. A. Pinto, J. Groenen, B. Zhao, T. Zhu, P. Sciau, Chromogenic mechanisms in blue-and-white porcelain. J. Eur. Ceram. Soc. 40 (15) (2020) 6181–6187. DOI :10.1016/j.jeurceramsoc.2020.06.065

41. T. Wang, T.Q. Zhu, Z.Y. Feng, B. Fayard, E. Pouyet, M. Cotte, W. DE Nolf, P. Sciau, Synchrotron radiation-based multi-analytical approach for studying underglaze color: the microstructure of Chinese Qinghua blue decors (Ming dynasty), Analytica Chimica Acta 928 (2016), 20-31. DOI: 10.1016/j.aca.2016.04.053

42. Zhang, F. The origin and development of traditional Chinese glazes and decorative ceramics color. In *Ancient Technology to Modern Science*; Kingery, W.D., Ed.; The American Ceramic Society, Colombus, OH, USA, 1985; Volume 1, pp. 163–180.

43. P. Colomban, G. Sagon, L.Q. Huy, N.Q. Liem, L. Mazerolles, Vietnamese (15th Century) Blue-and-White, Tam Thai and luster porcelains/stonewares: Glaze composition and decoration techniques, Archaeometry 46 (1) (2004) 125-136.

44. R. Wen, C.S. Wang, Z.W. Mao, Y.Y. Huang, A.M. Pollard, The chemical composition of blue pigment on Chinese blue-and-white porcelain of the Yuan and Ming Dynasties (AD 1271–1644). *Archaeometry* **2007**, *49*, 101–115.

45. Y.H. Zhou, Y.J. Hu, Y. Tao, J. Sun, Y. Cui, K. Wang, D.B. Hu, Study on the microstructure of the multilayer glaze of the 16th-17th century export blue-and-white porcelain excavated from Nan'ao Shipwreck, Ceram. Int. 42 (15) (2016) 17456-17465.

DOI :10.1016/j.ceramint.2016.08.050

46. R. Zhang, I. Garachon, P. Gethin, J. van Campen, Double layers glaze analysis of the Fujian export blue-and-white porcelain from the Witte Leeuw shipwreck (1613), Ceram. Int. 46 (9) (2020) 13474-13481. DOI :10.1016/j.ceramint.2020.02.131

47. E. de Pauw, P. Track, E. Verhaeven, S. Bauters, L. Acke, B. Vekemans, L. Vincze, Microbeam X-ray fluorescence and X-ray absorption spectroscopic analysis of Chinese blue-and-white porcelain dating from the Ming dynasty, Spectrochim. Acta Part B 149 (2018) 190-196.

Doi:10.1016/j.sab.2018.08.006

48. Kraak porcelain: The rise of global trade in the late 16th and early 17th centuries, L. Vinhals & J. Welsh Eds, 2008, Jorgue Welsh Books, London

Table 1. Information and visual characteristics of shards from Portuguese shipwrecks along the

South-Africa and Kenya coasts

Shipwreck (label)	Date	Place	Blue décor	Gloss	Decorative motif (after ref.2)
Saõ Jaõ Port Edward (SJ PE)	1552	Port Edward (Southern Natal)	Blue and dark blue;	Celadon-like glaze; medium; pits	Ming Dynasty, Jiajing Period (1522-1566 AD)
Saõ Jaõ Port Shepstone (SJ PS)	1552	Port Shepstone (Southern Natal)	Dark blue; Blue on body	poor	
Santo Alberto (SA)	1593 Exhibits features of Kraak ware	Sunrise-on-sea, Between Haga-Haga and Black Rock, Morgan's Bay (Eastern Cape)	Blue and dark blue; Black spots	poor	Early Wanli Period (1573-1622 AD) of the Ming Dynasty (1368 -1644 AD) Early Kraak ware
(SAb) (outgoing ship) Combine with Santo Alberto		Morgan's Bay (Eastern Cape)	Blue and dark blue; Blue on body	Poor	Early Wanli Period (1573-1622 AD) of the Ming Dynasty (1368 -1644 AD) Early Kraak ware
Mombasa	1630? Kraakware	Mombasa (Kenya)	Kraak ware; Blue on body	high	Kraak ware
Santa Maria Madre de Deus (SMMD)	1643	Bonza Bay, East London (Eastern Cape)	a1: Light blue a2,a3,a4: blue and light blue, dark spots	No gloss	Kraak ware, after 1600 AD
			b1,b3: light blue	No gloss	
			b2: blue and light blue	poor	
			b4: Light blue (Kraak ware ?)	High gloss	
Nostra Senhora da Atalaya do Pinheiro (NS)	1674	Cefané, north of East London (Eastern Cape)	Blue and dark blue; black spots Blue on body	No gloss	Kraak ware, after 1600 AD

Table 2 : Compositions

Table 2a: body composition

Sample/Oxide	SiO$_2$	Al$_2$O$_3$	MgO	Na$_2$O	K$_2$O	CaO	TiO$_2$	Fe$_2$O$_3$	MnO$_2$	CoO	CuO	Cl$_2$O
SJ PE	75.9	19.3	0.7	1.5	1.6	0.3	0.07	0.2	0.02	0.02	0.05	0.2
SJ PS	73.7	20.9	0.7	2.1	2.0	0.15	0.03	0.25	0.04	0.03	0.03	0.06
SA	70.2	24.8	0.5	1.9	1.6	0.3	0.05	0.3	0.07	0.03	0.03	0.06
SAb	64.6	27.9	0.9	2.3	3.0	0.2	0.1	0.7	0.08	0.03	0.04	0.03
SMMDa4	68.3	24.7	0.6	1.6	2.7	0.7	0.1	0.7	0.1	0.06	0.1	0.24
SMMDb4	68.0	26.0	0.8	2.3	2.0	0.3	0.04	0.3	0.04	0.04	0.04	0.06
SMMDb1	67.3	26.9	0.8	2.0	1.9	0.5	0.04	0.3	0.06	0.03	0.05	0.01
NS	69.8	24.7	0.8	1.4	1.2	0.9	0.2	0.5	0.09	0.04	0.15	0.12
Mombasa	64.0	30.4	0.6	1.5	2.3	0.3	0.1	0.5	0.08	0.07	0.08	0.02

Table 2b: Colourless glaze composition

Sample/Oxide	SiO$_2$	Al$_2$O$_3$	MgO	Na$_2$O	K$_2$O	CaO	TiO$_2$	Fe$_2$O$_3$	MnO$_2$	CoO	CuO	Cl$_2$O
SJ PE	69.6	20.6	1.3	2.5	1.1	3.9	0.05	0.3	0.07	0.06	0.15	0.2
SJ PS	73.7	16.0	0.3	3.4	2.6	3.2	0.04	0.4	0.03	0.06	0.08	0.1
SA	72.4	18.8	0.6	2.8	2.0	2.3	0.04	0.5	0.3	0.1	0.1	0.09
SAb	-	-	-	-	-	-	-	-	-	-	-	-
SMMDa4	74.8	16.8	0.2	2.7	2.0	2.9	0.06	0.3	0.05	0.05	0.08	0.07
SMMDb4	70.3	18.6	0.6	2.8	1.8	5.1	0.04	0.3	0.1	0.02	0.08	0.06
SMMDb1												
NS	-	-	-	-	-	-	-	-	-	-	-	-
Mombasa	71.6	20.5	0.6	2.3	1.9	2.0	0.05	0.5	0.2	0.08	0.1	0.17

Table 2c: Blue glaze composition.

Sample/Oxide	SiO$_2$	Al$_2$O$_3$	MgO	Na$_2$O	K$_2$O	CaO	TiO$_2$	Fe$_2$O$_3$	MnO$_2$	CoO	CuO	Cl$_2$O
SJ PE surface	67.4	16.9	0.8	1.3	3.0	7.9	0.07	0.95	1.2	0.25	0.1	0.15
SJ PE	68.2	17.6	0.6	1.4	2.7	7.1	0.08	0.8	1.1	0.17	0.15	0.09
SJ PS	71.6	18.3	0.5	3.4	2.3	2.4	0.06	0.4	0.8	0.1	0.09	0.07
SA	65.6	25.4	0.6	2.9	1.4	1.9	0.1	0.4	1.4	0.09	0.03	0.07
SAb	68.3	20.8	0.6	3.0	2.3	2.7	0.06	0.7	1.3	0.2	0.1	0.04
SMMDa4	73.2	15.2	0.4	2.5	3.1	3.3	0.07	0.9	0.6	0.1	0.1	0.7
SMMDa4 (interface)	72.9	16.2	0.3	2.4	2.9	2.7	0.1	0.7	1.0	0.1	0.18	0.4
SMMDb4	66.5	21.7	0.6	2.4	2.1	5.5	0.08	0.45	0.4	0.09	0.15	0.04
SMMD b1 (Interface)	61..3	28.1	0.6	2.1	2.7	3.6	0.07	0.7	0.5	0.13	0.1	0.015
SMMD b1 (surface)	67.6	18.6	0.5	2.5	2.4	6.8	0.09	0.6	0.7	0.06	0.14	0.02
NS	66.0	22.0	0.9	2.2	1.4	4.3	0.4	0.8	1.3	0.2	0.2	0.1
Mombasa	72.2	19.5	0.6	2.2	2.1	2.1	0.07	0.4	0.4	0.04	0.15	0.17

Fig. 1. Shards from a) São Jão (1552, Port Edward and Port Shepstone), Santa Maria Madre de Deus (1643, 4 samples), Santo Alberto (1593), Nostra Senhora da Atalia do Pinheiro (1647), and b) Santo Alberto b (1593?, 4 samples) and Santa Maria Madre de Deus (1643).

Fig. 2. Representative view of section of São Jão P.E. and P.S., Santo Alberto, Santo Alberto b, Santa Maria Madre de Deus (b4), Nostra Senhora and Mombasa shipwreck shards.

Fig. 3. Representative Raman spectra recorded on the body of shard section of Santa Madre de Deus (samples a1 and b3), Santo Alberto, São Jão P.E. and Nostra Senhora shipwreck shards (main peaks of quartz (q), mullite (m) and carbon (C) are labelled).

Fig. 4. Representative Raman spectra recorded on the colourless and blue glaze section of Nostra Senhora (NS), Santa Madre de Deus (samples b4, a1 and b3), Santo Alberta, and São Jão P.S. shipwreck shards.

Fig. 5. Representative Raman spectra recorded on dark blue glaze surface and black spots of Santa Madre de Deus (samples b4, recorded with both 455 and 532 nm lines) and Nostra Senhora blue and colourless glaze shipwreck shards. A baseline has been subtracted for spectra recorded under the 532 nm excitation.

Fig. 6: Optical view of a black spot (Santa Maria Madre de Deus b4 shipwreck sherd).

Fig. 7. Sequence of spectra measurements on section from the paste to the surface of the glaze: a) (low Ca glaze) Mombasa, b) Santo Alberto b (Ca medium-rich glaze) and c) Santa Maria Madre de Deus b4 (Ca-rich glaze) sherd.
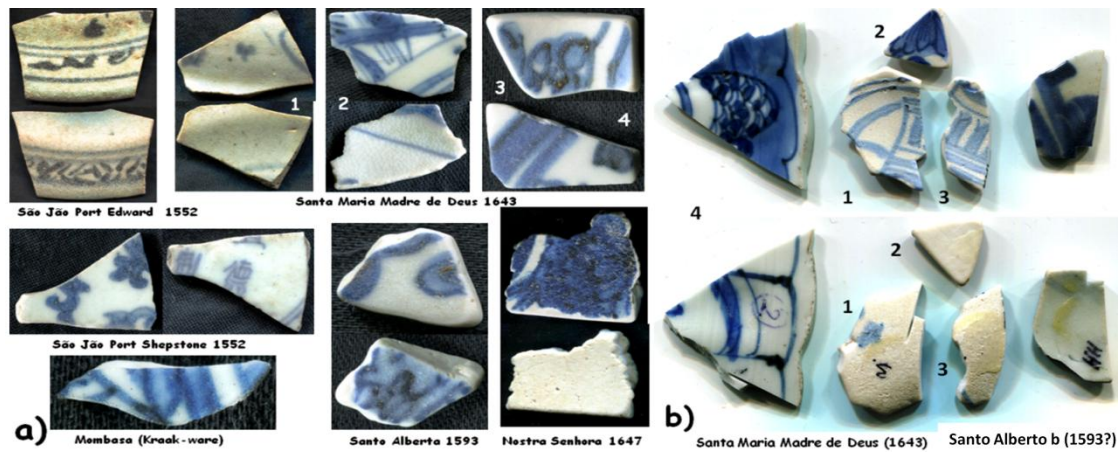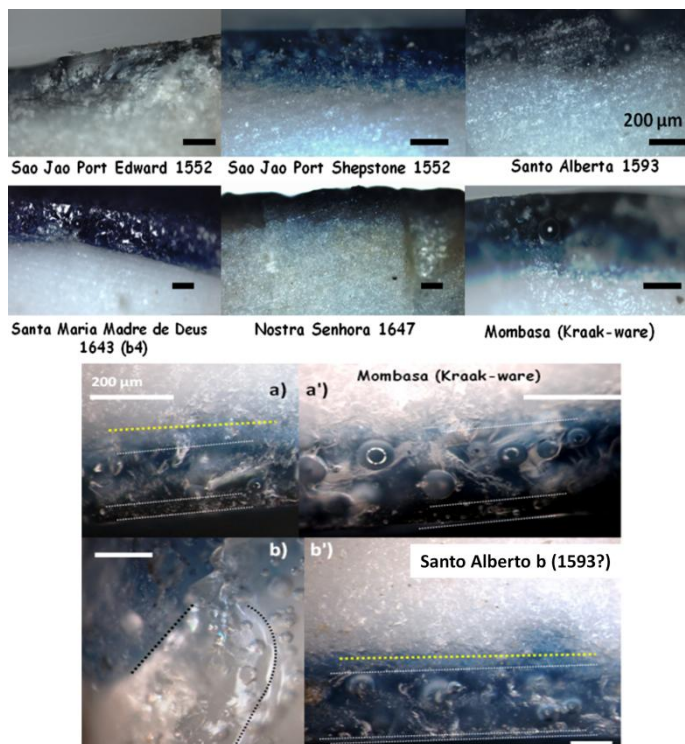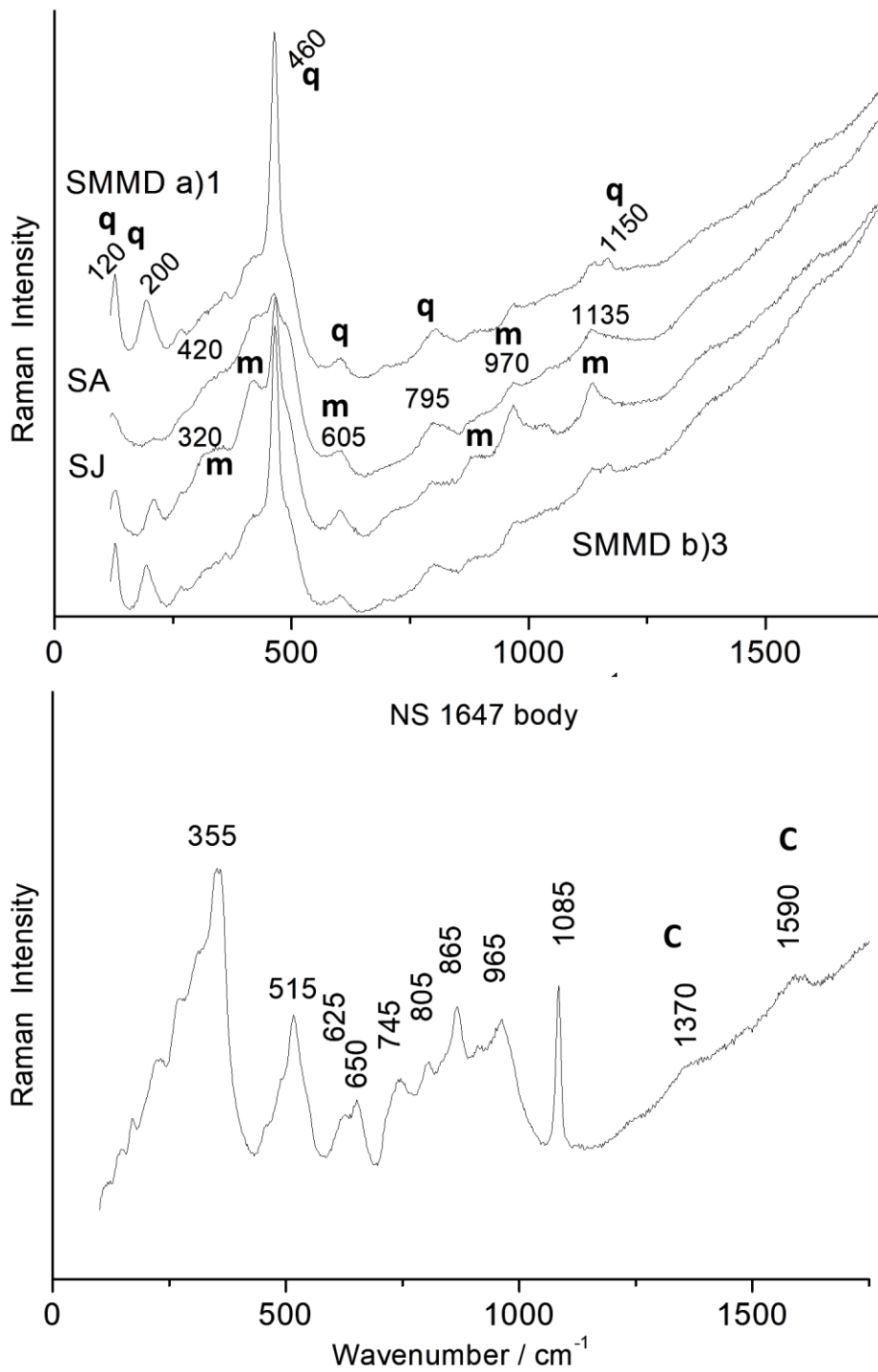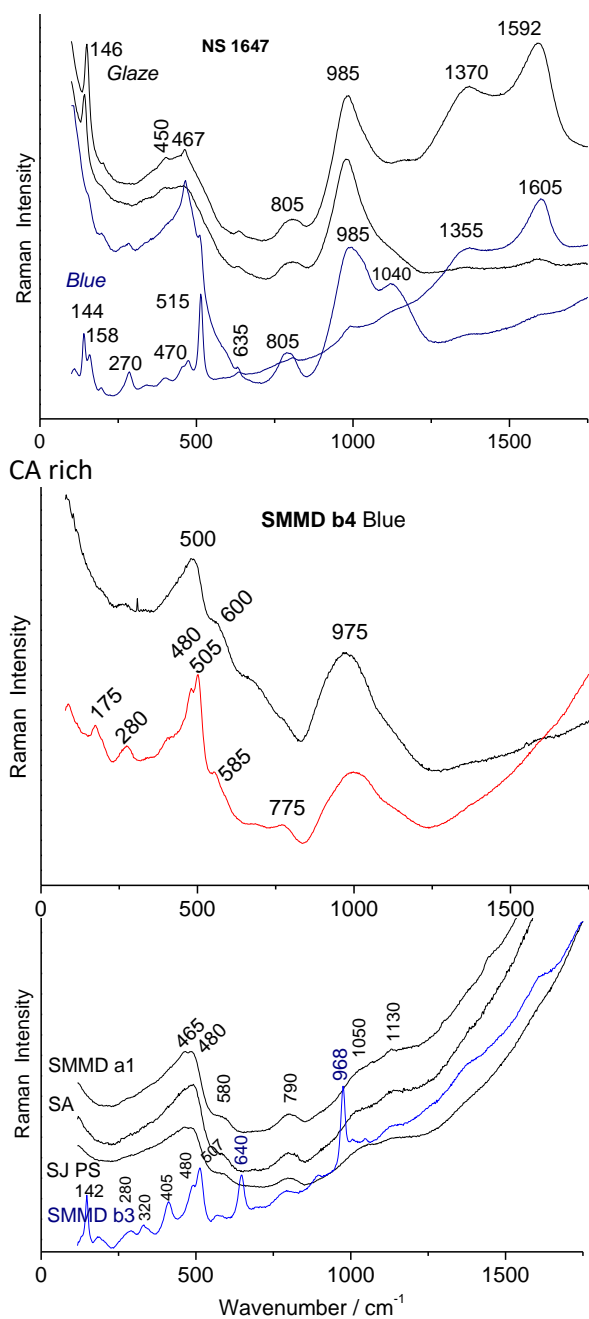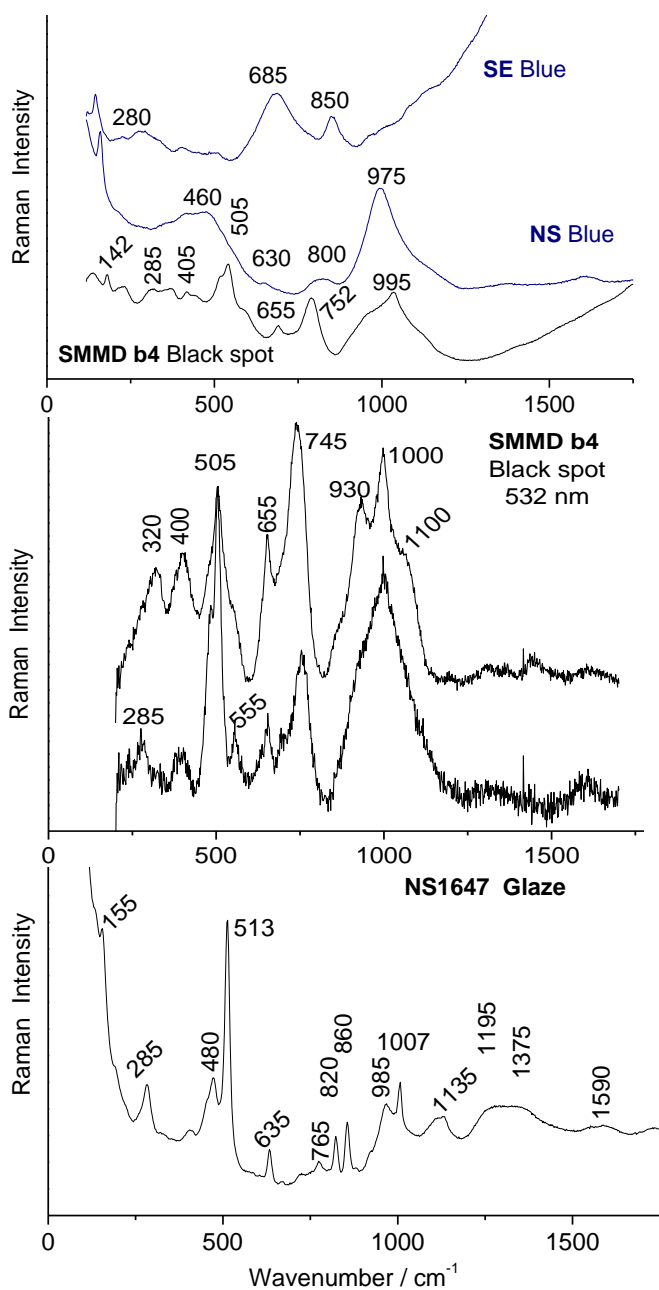
Fig. 1. Shards from a) São Jão (1552, Port Edward and Port Shepstone), Santa Maria Madre de Deus (1643, 4 samples), Santo Alberto (1593), Nostra Senhora da Atalia do Pinheiro (1647), and b) Santo Alberto b (1593?, 4 samples) and Santa Maria Madre de Deus (1643).

Fig. 2. Representative view of section of São Jão P.E. and P.S., Santo Alberto, Santo Alberto b, Santa Maria Madre de Deus (b4), Nostra Senhora and Mombasa shipwreck shards.

Fig. 3. Representative Raman spectra recorded on the body of shard section of Santa Madre de Deus (samples a1 and b3), Santo Alberto, São Jão P.E. and Nostra Senhora shipwreck shards (main peaks of quartz (q), mullite (m) and carbon (C) are labelled).

Fig. 4. Representative Raman spectra recorded on the colourless and blue glaze section of Nostra Senhora (NS), Santa Madre de Deus (samples b4, a1 and b3), Santo Alberto, and São Jão P.S. shipwreck shards.

Fig. 5. Representative Raman spectra recorded on dark blue glaze surface and black spots of Santa Madre de Deus (samples b4, recorded with both 455 and 532 nm lines) and Nostra Senhora blue and colourless glaze shipwreck shards. A baseline has been subtracted for spectra recorded under the 532 nm excitation.

Fig. 6: Optical view of a black spot (Santa Maria Madre de Deus b4 shipwreck sherd).

Fig. 7. Sequence of spectra measurements on section from the paste to the surface of the glaze: a) (low Ca glaze) Mombasa, b) Santo Alberto b (Ca medium-rich glaze) and c) Santa Maria Madre de Deus b4 (Ca-rich glaze) sherd.

Raman identification of the different glazing technologies of Blue-and-White Ming porcelains

Philippe Colomban[1*], Anh-Thu Ngo[1], Howell G.M. Edwards[2], Linda C Prinsloo[3], L. Valérie Esterhuizen[4]

[1] Sorbonne Université, CNRS, MONARIS umr8233, 4 Place Jussieu, 75005 Paris, France

[2] School of Chemistry and Biosciences, Faculty of Life Sciences, University of Bradford, Bradford, West Yorkshire BD18 4JX, United Kingdom

[3] Evolutionary Studies Institute, University of the Witwatersrand, PO WITS 2050, South Africa.

[4] Independent researcher, 287 Pleiades Ave, Waterkloof Ridge, Pretoria, 0181

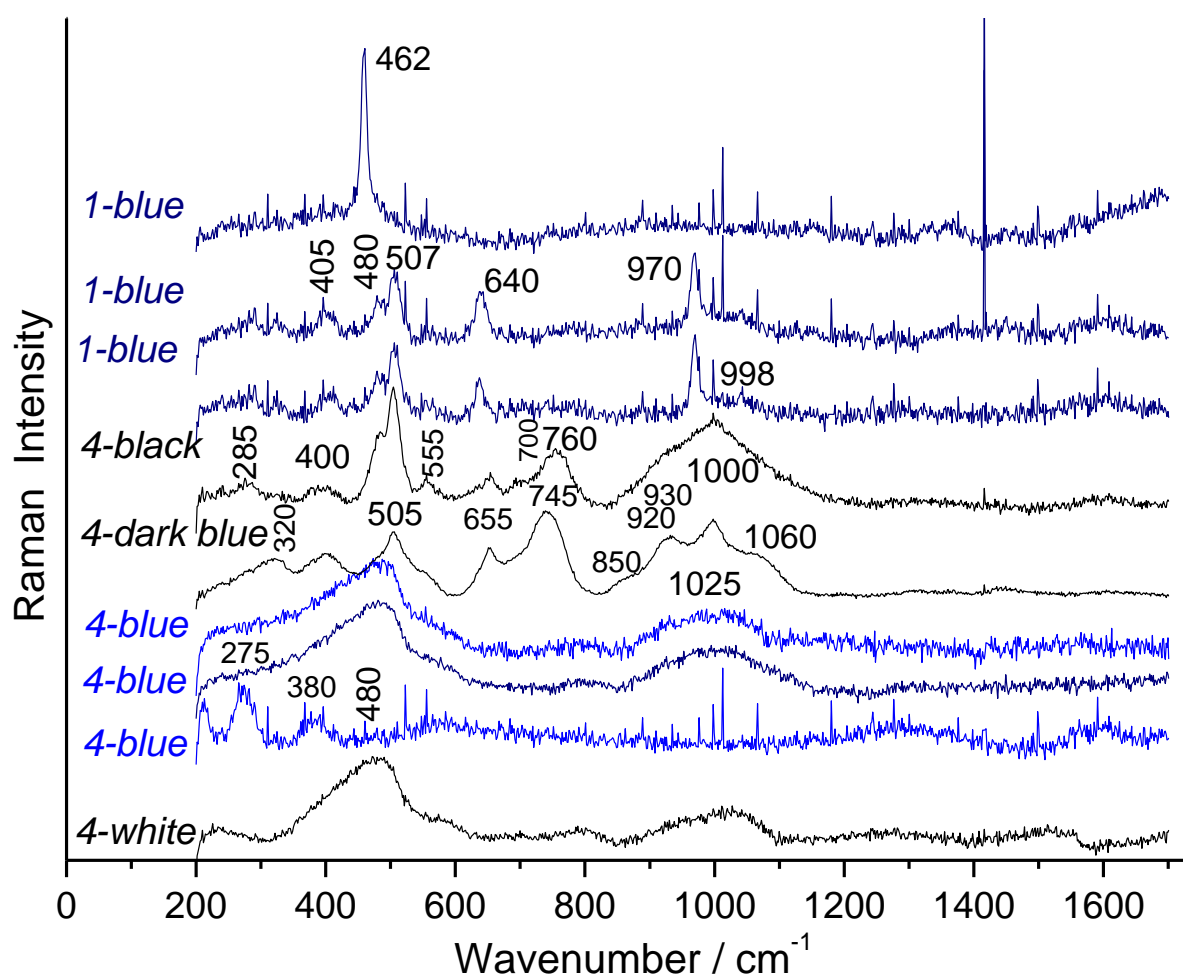*corresponding author philippe.colomban@sorbonne-universite.fr

Fig. S1. Representative Raman spectra recorded on the colourless (white), black and blue glaze of Santa Madre de Deus (samples a1 and a4) using 532 nm exciting laser line (LABRAM Infinity). A baseline has been subtracted.
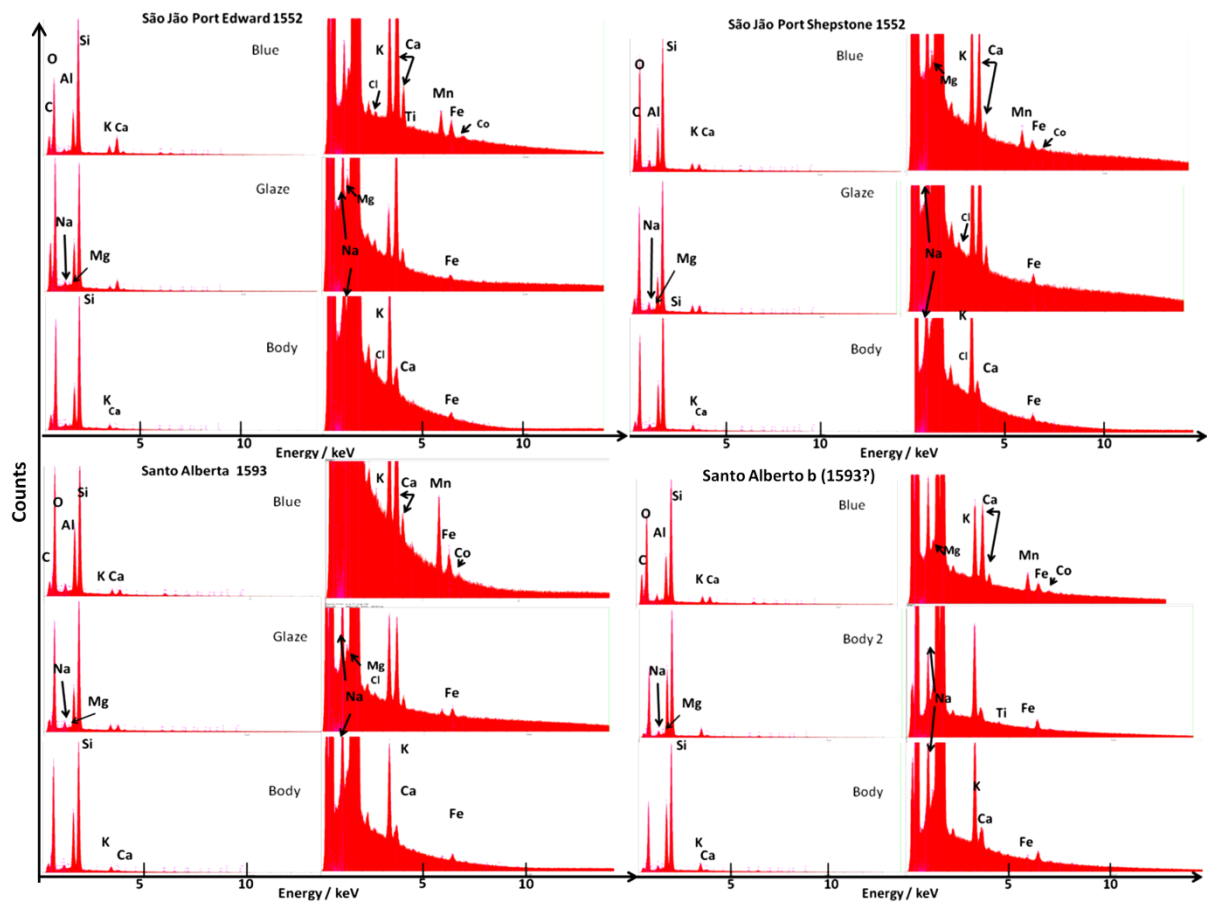
Fig. S2. Representative EDXS spectra recorded on the section of São João (P.E. and P.S.), Santo Alberto and Santo Alberto b shipwreck shards. A zoom is shown for the middle energy range in order to compare the signal of transition metals.
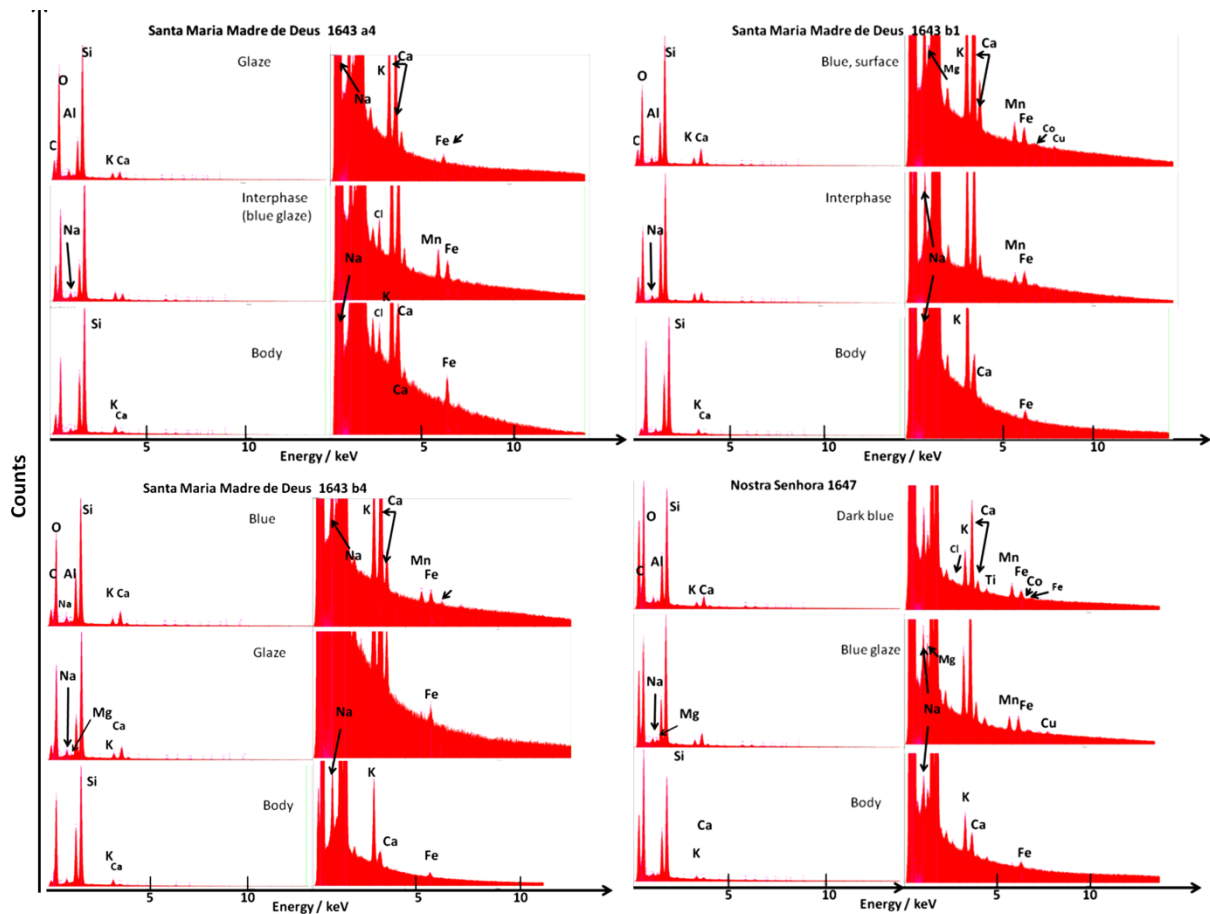
Fig. S3. Representative EDXS spectra recorded on the section of Santa Madre de Deus (samples a2, a1 and b4) and Nostra Senhora shipwreck shards. A zoom is shown for the middle energy range in order to compare the signal of transition metals.
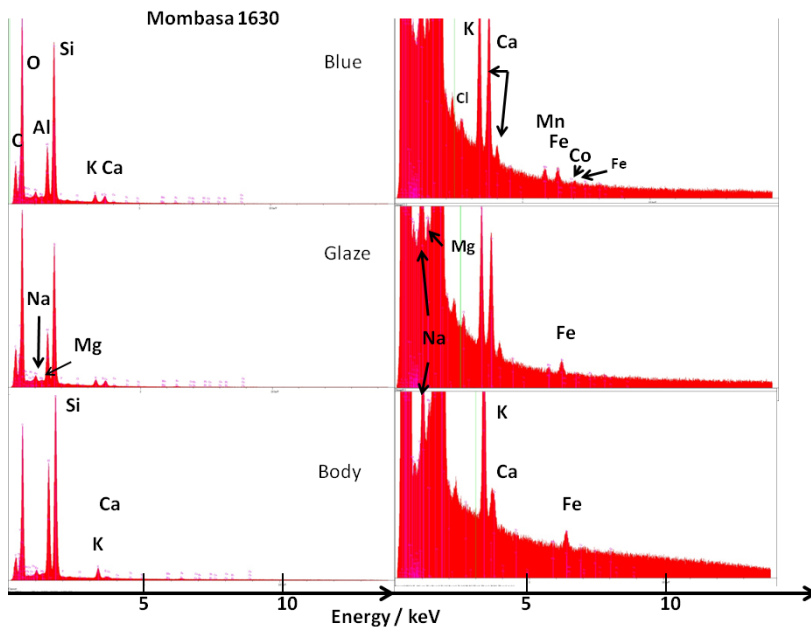

Fig. S4. Representative EDXS spectra recorded on the section of Mombasa shipwreck shard. A zoom is shown for the middle energy range in order to compare the signal of transition metals.